

Ca impurity in small mixed ^4He - ^3He clusters

R. Guardiola,¹ J. Navarro,¹ D. Mateo,² and M. Barranco²

¹*IFIC (CSIC-Universidad de Valencia),*

Apartado Postal 22085, E-46.071-Valencia, Spain

²*Departament E.C.M., Facultat de Física, and IN²UB,*

Universitat de Barcelona. Diagonal 647, E-08028 Barcelona, Spain

(Dated: February 4, 2022)

Abstract

The structure of small mixed helium clusters doped with one calcium atom has been determined within the diffusion Monte Carlo framework. The results show that the calcium atom sits at the ^4He - ^3He interface. This is in agreement with previous studies, both experimental and theoretical, performed for large clusters. A comparison between the results obtained for the largest cluster we have considered for each isotope shows a clear tendency of the Ca atom to reside in a deep dimple at the surface of the cluster for ^4He clusters, and to become fully solvated for ^3He clusters. We have calculated the absorption spectrum of Ca around the $4s4p \leftarrow 4s^2$ transition and have found that it is blue-shifted from that of the free-atom transition by an amount that depends on the size and composition of the cluster.

PACS numbers: 36.40.-c, 33.20.Kf, 67.60.gj

I. INTRODUCTION

Helium clusters are weakly bound quantum systems as a consequence of the small atomic mass and the weak van der Waals interaction between helium atoms. There are several recent papers [1, 2, 3, 4, 5, 6] reviewing the most relevant aspects of the physics and chemistry of these remarkable systems, to which we refer the interested reader.

It was found about twenty years ago that helium clusters could pick up closed shell molecules singly and that these molecules were located in the interior of the clusters [7, 8]. It is now well established that helium clusters may virtually capture any kind of atoms and molecules, most of which are located in their bulk. Alkali atoms are the sole known exception, as they remain on the surface of the cluster upon their capture. Electronic spectroscopy allows to obtain information on the cluster structure, and in particular on the position of embedded impurities in the cluster, via the shift and width of the electronic transitions [3, 9].

Heavy alkaline-earth atoms but magnesium exhibit a different behavior for each helium isotope, in contrast with most impurities, which solvate similarly in both. They are solvated in ^3He but not in ^4He clusters, in which case they reside in dimples on the cluster surface. Although still debated, the magnesium atom is most likely in a very delocalized state within the bulk of the ^4He cluster.

Clusters formed by a mixture of both helium isotopes are particularly interesting, as they are made of bosons and fermions with different mass interacting through the same potential. It is known that in the bulk, the excess in kinetic energy pushes the ^3He atoms to the liquid surface [10], an effect that also shows up in mixed droplets, see *e.g.* Ref. 11. It has been experimentally found that, depending on the size and composition of the drop, Ca atoms reside in bubbles at or near the ^4He - ^3He interface [12]. This scenario has been confirmed by density functional (DF) calculations [12, 13]. Heavy alkaline-earth atoms thus may offer a unique opportunity to study the interface of isotopically mixed helium clusters [14].

In this paper we address the study of small mixed ^4He - ^3He clusters doped with one Ca atom. Our calculations are based on diffusion Monte Carlo (DMC) methods using current realistic interatomic interactions. In particular, we have calculated density distribution functions and have estimated the atomic shifts and widths for Ca attached to a cluster, for several combinations of the number of isotopes in it. Results for some ^4He and ^3He clusters

doped with Ca are also presented to complete the discussion. It is worth stressing that, while ^4He clusters doped with different impurities have been thoroughly studied, theoretical works on doped ^3He clusters are scarce [15, 16, 17, 18, 19] apart from those carried out within the DF approach. The paper is organized as follows. In Sec. II we give some details about the DMC calculations. In Sec. III we present our results, and in Sec. IV we present a brief summary.

II. METHOD

The DMC description is based on a variational or importance sampling wave function. We have used a rather simple form, which contains the basic required properties. It is a generalization of the trial function adopted in our previous studies on pristine mixed helium clusters [20, 21]. It is written as a product of seven terms

$$\Psi(\mathcal{R}) = \Psi_{44} \Psi_{33} \Psi_{34} \Psi_{4\text{Ca}} \Psi_{3\text{Ca}} D_{\uparrow} D_{\downarrow} \quad (1)$$

consisting of a Jastrow factor for each pair of different atoms, plus the spin-up and -down Slater determinants required to satisfy the Pauli exclusion principle for ^3He fermions. Here $\{\mathcal{R}\}$ represents the set of $3(N_4 + N_3 + 1)$ coordinates of the atoms forming the cluster. Any of the Jastrow terms has the generic form

$$\Psi_{MN} = \prod_{i \neq j} \exp \left(-\frac{1}{2} \left[\frac{b_{MN}}{r_{ij}} \right]^{\nu_{MN}} - \alpha_{MN} r_{ij} \right), \quad (2)$$

where indices i, j run over the corresponding type of atom, and includes a short-range repulsion term with parameters b_{MN} and ν_{MN} associated to it, and a long-range confining term with corresponding parameter α_{MN} . The so defined Ψ_{MN} function is explicitly symmetric under the exchange of particles.

The antisymmetry required for ^3He fermions is incorporated in the Slater determinants D_{\uparrow} and D_{\downarrow} , related to the spin-up and -down fermions. These Slater determinants are of primary relevance because they define the set of spin-up and -down nodal surfaces which strongly constrain the DMC algorithm. As in our previous works [20, 21] we have assumed a shell-model like structure, taking the single-particle orbitals as harmonic polynomials of the fermionic cartesian coordinates, thus guaranteeing that the resulting Slater determinants are translationally invariant. Moreover, we have always assumed a filling scheme in which

the total spin is minimum, either 0 or 1/2, respectively, for N_3 even or odd. Also, the so called Feynman-Cohen back-flow [22] has been incorporated into the scheme by substituting

$$\mathbf{r}_i \rightarrow \tilde{\mathbf{r}}_i = \mathbf{r}_i + \sum_{i \neq j} \eta(r_{ij})(\mathbf{r}_i - \mathbf{r}_j) \quad (3)$$

in the Slater determinants [23]. For the backflow function $\eta(r)$ we choose the medium-range form used in Ref. 24, namely $\eta(r) = \lambda/r^3$, with the same value of $\lambda = 5 \text{ \AA}^3$.

The form of the short-range repulsion term was introduced long ago by McMillan [25] for describing the homogeneous liquid ^4He using a 12-6 Lennard-Jones interaction. The values of the two parameters ν and b are fixed by the short-range behavior of a pair of atoms. In our calculations we have employed the He-He Aziz HFD-B(HE) [26] potential, and that of Hinde [27] for the $X^1\Sigma$ Ca-He interaction, as parametrized in Ref. 13. For all cluster sizes we have used the following values: $\nu_{MN} = 5.2 \text{ \AA}$, $b_{44} = 2.95 \text{ \AA}$, $b_{33} = 2.85 \text{ \AA}$, $b_{34} = 2.90 \text{ \AA}$, as in previous works on pristine and isotopically mixed helium clusters, and $b_{4\text{Ca}} = 3.25 \text{ \AA}$, and $b_{3\text{Ca}} = 3.00 \text{ \AA}$. Thus, the trial or importance sampling wave function contains only five free parameters, namely α_{44} , α_{33} , α_{34} , $\alpha_{4\text{Ca}}$, and $\alpha_{3\text{Ca}}$, which have been determined by minimizing the expectation value of the Hamiltonian.

For the DMC algorithm we have used the short-time Green function approximation [28, 29] with an $O(\tau^3)$ form [30]. It is worth mentioning that this approximate Green function satisfies the microreversibility condition (detailed balance condition). Moreover, the random process was constrained so as not to traverse the nodal surfaces, using the so called fixed node approximation.

III. RESULTS

A. Structure and energetics of $\text{Ca}@^4\text{He}_{N_4} + ^3\text{He}_{N_3}$ clusters

In Figures 1-4 are plotted the densities in the $y = 0$ plane of the $(N_4, N_3) = (20, 20)$, $(20, 8)$, $(8, 20)$, and $(8, 8)$ clusters. After a simulation running for a long thermalization time we have stored a large number of walkers (typically 10^6) to get a mixed estimator of the probability densities. A series of angular rotations have been performed on each walker to place the Ca atom on the z -axis, defined as the line joining the impurity and the cluster center-of-mass. Afterwards, a projection on the $y = 0$ plane has been performed. The

resulting plots thus exhibit axial symmetry.

These clusters display an already well known structure, with a core of ^4He atoms surrounded by a shell of ^3He atoms. Interestingly, in spite of the small number of helium atoms, the tendency of Ca to reside at the ^4He - ^3He interface is clearly visible. Note also the peak in the ^4He densities near to Ca, and those appearing in the ^3He shell: the one near the impurity is reminiscent of the solvation shell that would fully develop in a larger cluster made of either kind of atoms. We attribute the ^3He peak distant from the impurity to the tendency of the ^3He atoms to reside, whenever possible, far from the impurity [31] because the Ca-He interaction is weaker than the He-He one. Within DF theory, a qualitatively similar structure has been found for clusters with $N_4 = 50$ and $N_3 = 18, 32, 50$, and 68 [13].

The calculated ground state energies of the clusters, as well as the solvation energy of the dopant, defined as

$$S(\text{Ca}) = E(\text{Ca}@^4\text{He}_{N_4} + ^3\text{He}_{N_3}) - E(^4\text{He}_{N_4} + ^3\text{He}_{N_3}) , \quad (4)$$

are given in Table I. We mention that Elhiyani and Lewerenz [32] have carried out calculations for $\text{Ca}@^4\text{He}_{N_4}$ clusters using the same He-He interaction than ours, and a Ca-He pair potential they have obtained at the CCSD(T) level of accuracy, as Hinde's one [27]. Their Ca solvation energies for clusters with $N_4 = 20$ and 40 are -12.29 (1) and -16.55 (6) K, respectively, in good agreement with ours as displayed in Table I.

In Fig. 5 are plotted the Ca solvation energies per helium atom as a function of the total number of helium atoms in the cluster. Note the conspicuous shell oscillations for $N_4 = 0$. We discuss them below.

B. The case of $\text{Ca}@^3\text{He}_{N_3}$ clusters

The study of the lightest ^3He clusters has a great interest, as they are a challenge for theoretical methods due to their very small binding energy. In particular, pure ^3He clusters are bound only for sizes greater than $N_3 \sim 30$ atoms [20, 33, 34], and small mixed ^4He - ^3He clusters present instability regions as a function of N_4 and N_3 [21, 35, 36]. It has been shown that the presence of one ^4He atom is enough to trigger the binding of twenty ^3He atoms [21], showing the importance of the zero-point motion in the stability of small helium clusters.

The Ca-He interaction potential is weaker than the He-He one, and its minimum lies at

a larger distance. Nevertheless, due to the different zero-point energy of Ca and He atoms, we have found that the presence of one single Ca atom causes that clusters made of any number of atoms are bound, irrespective of their bosonic or fermionic character. This is an obvious result for ^4He clusters, but it is not for ^3He clusters. We give in Table II the total energy of $\text{Ca}@^3\text{He}_{N_3}$ clusters, and have already represented them, divided by N_3 , in Fig. 5 ($N_4 = 0$ results) because as the pristine ^3He clusters are not bound, it makes sense to plot these energies together with the solvation energy of Ca discussed before. It is interesting to see the sharp minima at $N_3 = 2, 8$, and 20 . These numbers correspond to the first shell closures of the three-dimensional spherical harmonic oscillator, in spite that the helium density distributions are far from being spherical, especially for small N_3 values (see Fig. 7). We have no plausible explanation for this finding. However, it is worth recalling that in cylindrical symmetry [37], the first two minima also arise from the 1σ and $1\sigma, 2\sigma, 1\pi$ shell closures corresponding to this geometry, see *e.g.*, Ref. 13.

For $\text{Ca}@^3\text{He}_{N_3}$ clusters we may also calculate the differences

$$\Delta(N_3) = E(\text{Ca}@^3\text{He}_{N_3}) - E(\text{Ca}@^3\text{He}_{N_3-1}) \quad (5)$$

than can be interpreted as the negative of the He evaporation energies [38]. We have plotted $-\Delta(N_3)$ in Fig. 6. The large drops in the evaporation energy after $N_3 = 2, 8$, and 20 correlate well with the “magicity” of these values, i.e., with shell closures. In the $N_3 = 9 - 20$ range, the evaporation energy displays some structure, with a weak local maximum at $N_3 = 12$.

As representative examples, the density distributions in the $y = 0$ plane for the $\text{Ca}@^3\text{He}_{N_3}$ clusters with $N_3 = 2, 3, 4, 5, 8$, and 20 are plotted in Fig. 7. It can be clearly seen the tendency of the Ca atom to become solvated in ^3He clusters. It is also interesting to compare the morphology of ^4He and ^3He clusters doped with Ca. To this end, we have plotted in Fig. 8 the density distributions corresponding to helium clusters made of 40 atoms doped with it. It can be seen that Ca is in a dimple state on the surface of the ^4He cluster, whereas it moves towards the bulk of the cluster in the case of ^3He . In spite of this bulk location, the $\text{Ca}@^3\text{He}_{40}$ cluster is not spherically symmetric. This also happens for clusters doped with other weakly attractive impurities, such as Mg in small ^4He clusters [38]. The reason is the tendency of the system to have a helium density as close as possible to its liquid value in order to maximize its binding. This is easier to achieve in an off-center location for small clusters, even for $N_3 = 2$. In this case the two ^3He atoms are slightly apart as a consequence

of their large zero-point motion, not fully compensated by the attraction of the Ca impurity. This is the reason of the very low He density in a cylindrical region surrounding the z -axis, see the corresponding panel in Fig. 7, which is absent in the other clusters. Eventually, when the number of ^3He atoms increases, the center-of-masses of the helium moiety and the impurity nearly coincide [14].

C. Absorption spectrum of Ca in $^4\text{He}_{N_4} + ^3\text{He}_{N_3}$ clusters

The DMC calculation provides us with a set $\{\mathcal{R}\}$ of walkers indicating the instantaneous position of each atom in the cluster. From these walkers we have calculated the density distribution functions plotted in the previous subsections. Here we use them to obtain the absorption spectrum of the $4s4p\ ^1P_1 \leftarrow 4s^2\ ^1S_0$ transition in Ca.

Electronic spectroscopy is a powerful tool to disclose the structure of impurities in helium clusters, since the shift and width of the electronic transitions is very sensitive to the dopant environment [3, 5]. Lax method [39] has been since long time ago the standard way to determine the absorption spectrum of a dopant atom in helium clusters. It makes use of the Franck-Condon principle within a semiclassical approach. It has been adapted and used by several authors to analyze the absorption spectrum of *e.g.*, lithium in solid H_2 [40], and of different atoms in helium clusters [41, 42, 43, 45]. The particular case of Ca atoms we are interested in has been addressed within DF in pure and mixed helium clusters [12, 43]. Lax method is usually applied in conjunction with the diatomics-in-molecules approach [46], in which the atom-cluster complex is treated as a diatomic molecule, the helium moiety playing the role of the other atom.

We have calculate the line shape of the electronic absorptium transition in Ca as

$$I(\omega) \propto \int d\mathcal{R} |\Psi_{gs}(\mathcal{R})|^2 \delta(\omega + V_{gs}(\mathcal{R}) - V_{ex}(\mathcal{R})) , \quad (6)$$

where $\{\mathcal{R}\}$ refers to the positions of the atoms, and V_{gs} and V_{ex} are, respectively, the ground and excited states potential energy surfaces. We have used the Ca-He $X^1\Sigma$ interaction of Ref. 27 for the ground state, and the $^1\Pi$ and $^1\Sigma$ potentials of Ref. 43 for the excited states. In short, for a given value of ω , a 3×3 matrix has to be diagonalized to determine the three components of the absorption line, each one arising from a different potential energy surface, i.e., eigenvalue of the excited energy matrix, see Refs. 43, 44 for the details.

In Fig. 9 is plotted the absorption spectrum of Ca for several combinations of N_4 and N_3 values. The energies are referred to the free Ca atom value (23650 cm^{-1}). For so few helium atoms, there is no appreciable shift, but an appreciable width increasing as N_3 does at fixed N_4 . A large enough number of walkers bear the information corresponding to a quasi-free Ca atom within the simulation volume. This is the reason of the narrow peak at $\omega = 0$. A similar peak appears in the experiments, and it is due to the excitation of gas-phase Ca atoms present in the doping chamber [47].

In Fig. 10 is plotted the absorption spectrum of Ca for three selected (N_4, N_3) combinations with $N_4 + N_3 = 40$. The contributions from the three potential energy surfaces are shown, and the long tail at high frequencies is identified as likely arising from the very repulsive contribution of the $^1\Sigma$ pair potential. The shift in the $(0, 40)$ case is clearly seen. Finally, in Fig. 11 we display the absorption spectrum of $\text{Ca}@^3\text{He}_{N_3}$ for increasing values of N_3 . Not surprisingly, the $N_3 = 2$ case shows no appreciable shift and a small width. As N_3 increases, both the shift and width progressively do.

IV. SUMMARY

Within the diffusion Monte Carlo framework, we have studied the structure and energetics of small mixed ^4He - ^3He clusters doped with Ca. We have found that a single Ca atom is able to produce bound clusters made of any number of helium atoms, irrespective of their fermionic or bosonic character. In the case of ^3He clusters, this is a somewhat unexpected result, as the Ca-He interaction is weaker than the He-He one. We attribute it to a zero-point motion effect.

We have found that Ca resides in a deep dimple at the surface of ^4He clusters, and in the bulk of ^3He clusters, in agreement with experiments carried out for large helium clusters [12, 47].

In the case of mixed clusters, our calculations show the tendency of the impurity to sit at the ^4He - ^3He interface, although the small number of fermions that we can microscopically handle does not allow us to make a clear distinction between the interface and the rest of the mixed cluster. Morphologically, we have found that doped mixed clusters obtained within DF theory [13] are qualitatively similar to those obtained within the microscopic DMC approach.

Finally, we have used the DMC walkers to semiclassically obtain the absorption spectrum of Ca around the $4s4p \leftarrow 4s^2$ transition, and have found that it is slightly blue-shifted from that of free-atom transition, with a clear dependence on the size and composition of the mixed cluster in spite of the small number of helium atoms in the studied systems. We want to mention that the excitation and emission spectra of Ca atoms implanted in liquid ^4He and ^3He have been measured [48], and that their determination in the case of liquid mixtures could also be carried out as a function of pressure and composition. We are at present extending the method implemented in Ref. [12] to address this issue.

Acknowledgments

We thank Alberto Hernando and Martí Pi for useful discussions and comments, and Mohamed Elhiyani and Marius Lewerenz for providing us with their results prior to publication. This work has been supported by Grants FIS2007-60133 and FIS2008-00421 from DGI, Spain (FEDER), and 2009SGR1289 from Generalitat de Catalunya.

-
- [1] J. P. Toennies and A. F. Vilesov, *Angew. Chem. Int. Ed.* **43**, 2622 (2004).
 - [2] M. Barranco, R. Guardiola, E. S. Hernández, R. Mayol, J. Navarro, and M. Pi, *J. Low Temp. Phys.* **142**, 1 (2006).
 - [3] F. Stienkemeier and K. K. Lehman, *J. Phys. B: At. Mol. Opt. Phys.* **39**, R127 (2006).
 - [4] M. Y. Choi, G. E. Douberly, T. M. Falconer, W. K. Lewis, C. M. Lindsay, J. M. Merrit, P. L. Stiles, and R. E. Miller, *Int. Rev. Phys. Chem.* **25**, 15 (2006).
 - [5] J. Tiggesbäumker and F. Stienkemeier, *Phys. Chem. Chem. Phys.* **9**, 4748 (2007).
 - [6] K. Szalewicz, *Int. Rev. Phys. Chem.* **27**, 273 (2008).
 - [7] A. Scheidemann, J. P. Toennies, and J. A. Northby, *Phys. Rev. Lett.* **64**, 1899 (1990).
 - [8] A. Scheidemann, B. Schilling, and J. P. Toennies, *J. Phys. Chem.* **97**, 2128 (1993).
 - [9] F. Stienkemeier and A. F. Vilesov, *J. Chem. Phys.* **115**, 10119 (2001).
 - [10] A. F. Andreev, *Sov. Phys. JETP* **23**, 939 (1966).
 - [11] M. Barranco, M. Pi, S. M. Gatica, E.S. Hernández, and J. Navarro, *Phys. Rev. B* **56**, 8997 (1997).

- [12] O. Bünermann, M. Dvorak, F. Stienkemeier, A. Hernando, R. Mayol, M. Pi, M. Barranco, and F. Ancilotto, *Phys. Rev. B* **79**, 214511 (2009).
- [13] D. Mateo, M. Barranco, R. Mayol, and M. Pi, *Eur. Phys. J. D* **52**, 63 (2009).
- [14] A. Hernando, R. Mayol, M. Pi, M. Barranco, F. Ancilotto, O. Bünermann, and F. Stienkemeier, *J. Phys. Chem. A* **111**, 7303 (2007).
- [15] P. Barletta, A. Fabrocini, A. Kievsky, J. Navarro, and A. Polls, *Phys. Rev. A* **68**, 053205 (2003).
- [16] D. López-Durán, M. P. de Lara-Castells, G. Delgado-Barrio, P. Villarreal, C. Di Paola, F. A. Gianturco, and J. Jellinek, *Phys. Rev. Lett.* **93**, 053401 (2004).
- [17] M. P. de Lara-Castells, G. Delgado-Barrio, P. Villarreal, and A. O. Mitrushchenkov, *J. Chem. Phys.* **125**, 221101 (2006).
- [18] M. P. de Lara-Castells, A. O. Mitrushchenkov, G. Delgado-Barrio, and P. Villarreal, *Few-Body Syst.* **45**, 233 (2009).
- [19] M. P. de Lara-Castells, P. Villarreal, G. Delgado-Barrio, and A. O. Mitrushchenkov, submitted to *J. Chem. Phys.* (2009).
- [20] R. Guardiola and J. Navarro, *Phys. Rev. Lett.* **84**, 1144 (2000).
- [21] R. Guardiola and J. Navarro, *Phys. Rev. Lett.* **89**, 193401 (2002).
- [22] R. P. Feynman and M. Cohen, *Phys. Rev.* **102**, 1189 (1956).
- [23] K. E. Schmidt, M. A. Lee, M. H. Kalos, and G. V. Chester, *Phys. Rev. Lett.* **47**, 807 (1981).
- [24] V. R. Pandharipande, S. C. Pieper, and R. B. Wiringa, *Phys. Rev. B* **34**, 4571 (1986).
- [25] W-L- McMillan, *Phys. Rev.* **138**, A442 (1965).
- [26] R. A. Aziz, F. R. McCourt and C. C. K. Wong, *Mol. Phys.* **61**, 1487 (1987).
- [27] R. J. Hinde, *J. Phys. B: At. Mol. Opt. Phys.* **36**, 3119 (2003).
- [28] J. B. Anderson, *J. Chem. Phys.* **73**, 3897 (1980).
- [29] P. J. Reynolds, D. M. Ceperley, B. J. Alder, and W. A. Lester Jr., *J. Chem. Phys.* **77**, 5593 (1982).
- [30] J. Vrbik and S. M. Rothstein, *J. Comput. Phys.* **63**, 130 (1986).
- [31] D. Mateo, M. Barranco, R. Mayol, J. Navarro, and M. Pi, *J. Phys. Conf. Ser.* **150**, 032051 (2009).
- [32] M. Elhiyani and M. Lewerenz, unpublished (2009).
- [33] M. Barranco, J. Navarro and A. Poves, *Phys. Rev. Lett.* **78**, 4729 (1997).

- [34] E. Sola, J. Casulleras, and J. Boronat, Phys. Rev. B **73**, 092515 (2006).
- [35] D. Bressanini and G. Morosi, Phys. Rev. Lett. **90**, 133401 (2003).
- [36] A. Kalinin, O. Kornilov, W. Schöllkopf, and J. P. Toennies, Phys. Rev. Lett. **95**, 113402 (2005).
- [37] In axial geometry, the projection of the angular momentum on the symmetry axis is the good quantum number, and single-particle states with angular momentum $\pm l_z$ are degenerate. Thus, taking into account the spin degeneracy, levels with $l_z = 0$ are twofold degenerate, and those with $l_z \neq 0$ are fourfold degenerate.
- [38] M. Mella, G. Calderoni, and F. Cargnoni, J. Chem. Phys. **123**, 054328 (2005)
- [39] M. Lax, J. Chem. Phys. **20**, 1752 (1952).
- [40] E. Cheng and K. B. Whaley, J. Chem. Phys. **104**, 3155 (1996)
- [41] A. Nakayama and K. Yamashita, J. Chem. Phys. **114**, 780 (2001)
- [42] M. Mella, M. C. Colombo, and G. Morosi, J. Chem. Phys. **117**, 9695 (2002)
- [43] A. Hernando, R. Mayol, M. Pi, and M. Krośnicki, Phys. Rev. B **77**, 024513 (2008).
- [44] A. Hernando, M. Barranco, R. Mayol, M. Pi, F. Ancilotto, O. Bünermann, and F. Stienkemeier, J. Low Temp. Phys. to be published, DOI 10.1007/s10909-009-9934-7 (2009).
- [45] A. Hernando, M. Barranco, R. Mayol, M. Pi, and F. Ancilotto, Phys. Rev. B **78**, 184515 (2009).
- [46] F. O. Ellison, J. Am. Chem. Soc. **85**, 3540 (1963).
- [47] F. Stienkemeier, F. Meier, and H. O. Lutz, J. Chem. Phys. **107**, 10816 (1997).
- [48] Y. Moriwaki and N. Morita, Eur. Phys. J. D **33**, 323 (2005).

TABLE I: Ground state energies (in units of K) of mixed helium clusters, pristine and Ca doped, and solvation energy of Ca for several combinations of N_4 and N_3 .

N_4	N_3	$E(^4\text{He}_{N_4} + ^3\text{He}_{N_3})$	$E(\text{Ca}@^4\text{He}_{N_4} + ^3\text{He}_{N_3})$	$S(\text{Ca})$
8	0	-5.086 (3)	-12.059 (4)	-6.973 (5)
8	8	-11.884 (14)	-22.286 (9)	-10.402 (17)
8	20	-20.514 (16)	-34.061 (20)	-13.547 (22)
20	0	-33.427 (10)	-45.752 (16)	-12.325 (19)
20	8	-46.705 (20)	-60.959 (25)	-14.254 (32)
20	20	-62.265 (41)	-78.634 (50)	-16.369 (65)
40	0	-101.935 (25)	-118.836 (14)	-16.901 (29)

TABLE II: Ground state energies of $\text{Ca@}^3\text{He}_{N_3}$ clusters

N_3	Energies (K)	N_3	Energies (K)	N_3	Energies (K)
1	-0.531 (1)	8	-4.168 (4)	15	-5.745 (8)
2	-1.120 (1)	9	-4.287 (4)	16	-6.333 (8)
3	-1.477 (2)	10	-4.449 (5)	17	-6.983 (9)
4	-1.885 (2)	11	-4.600 (6)	18	-7.705 (9)
5	-2.366 (3)	12	-4.789 (6)	19	-8.573 (9)
6	-2.906 (3)	13	-4.916 (7)	20	-9.410 (10)
7	-3.504 (3)	14	-5.193 (7)	21	-9.586 (24)

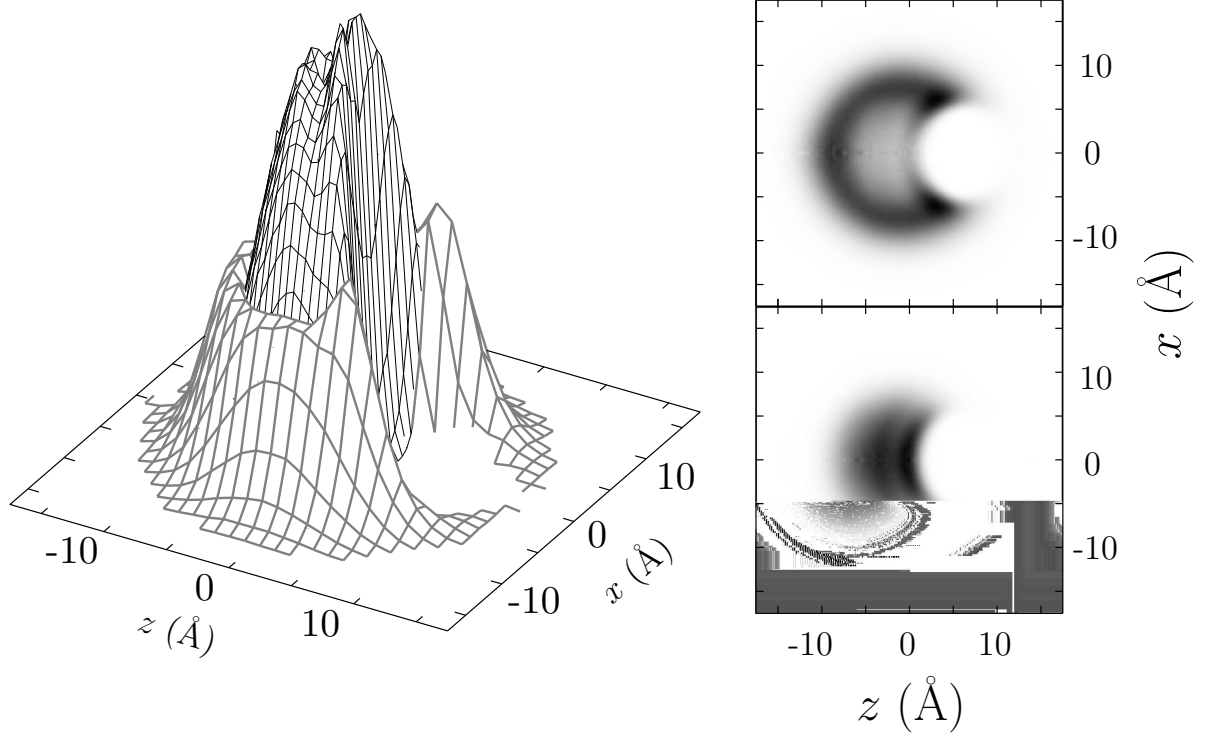


FIG. 1: Density distributions in the $y = 0$ plane for the $\text{Ca}@^4\text{He}_{20}+^3\text{He}_{20}$ cluster. Left: 3D representation. Right: grey scale plot of ^3He (top) and ^4He (bottom) densities. The darker the region, the higher the helium density.

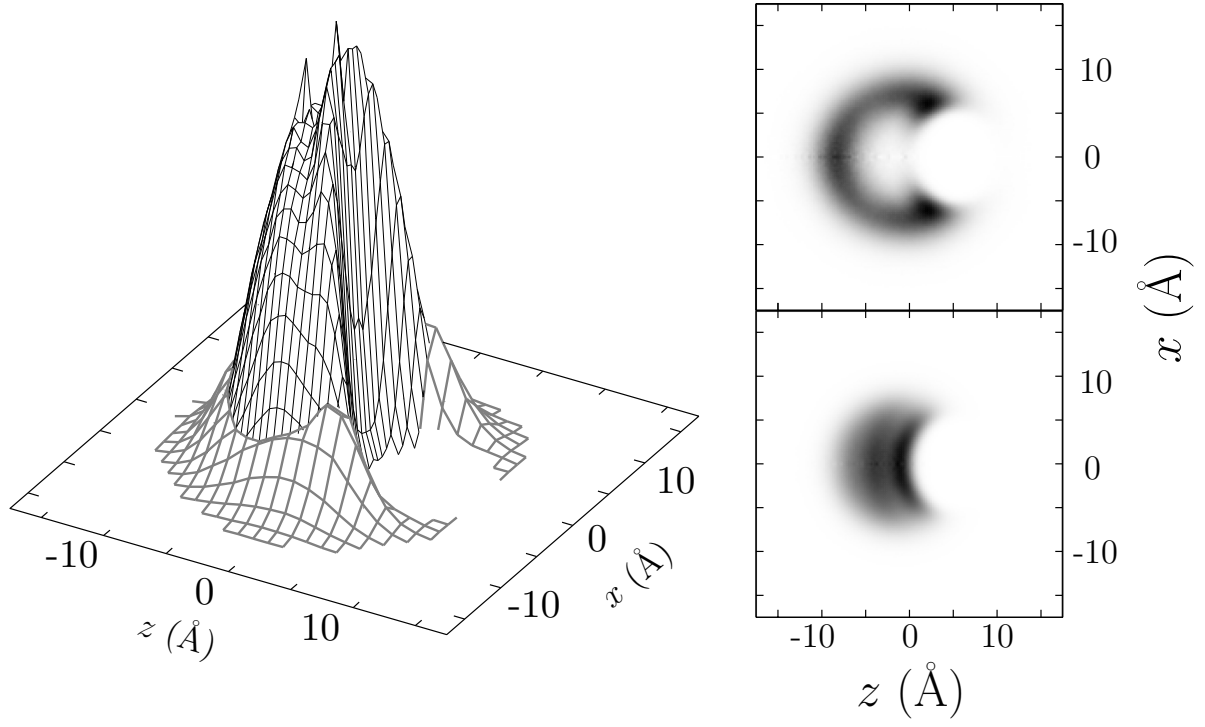


FIG. 2: Same as Fig. 1 for $N_4 = 20$, $N_3 = 8$.

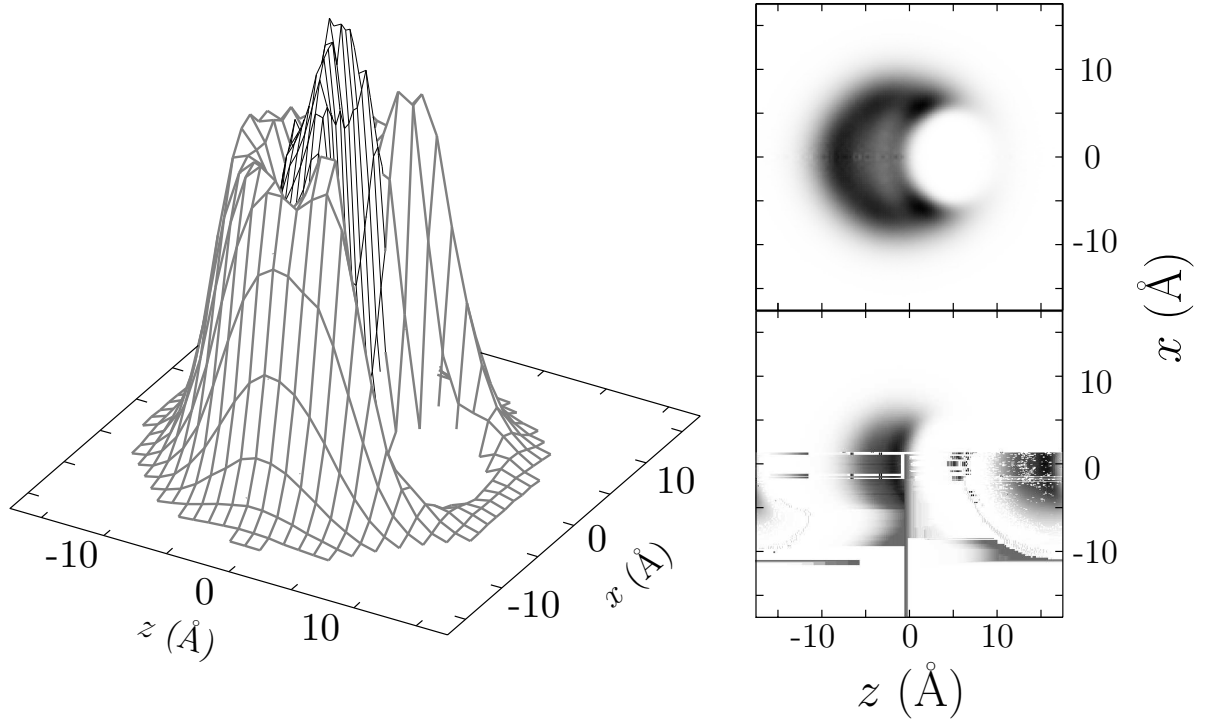


FIG. 3: Same as Fig. 1 for $N_4 = 8$, $N_3 = 20$.

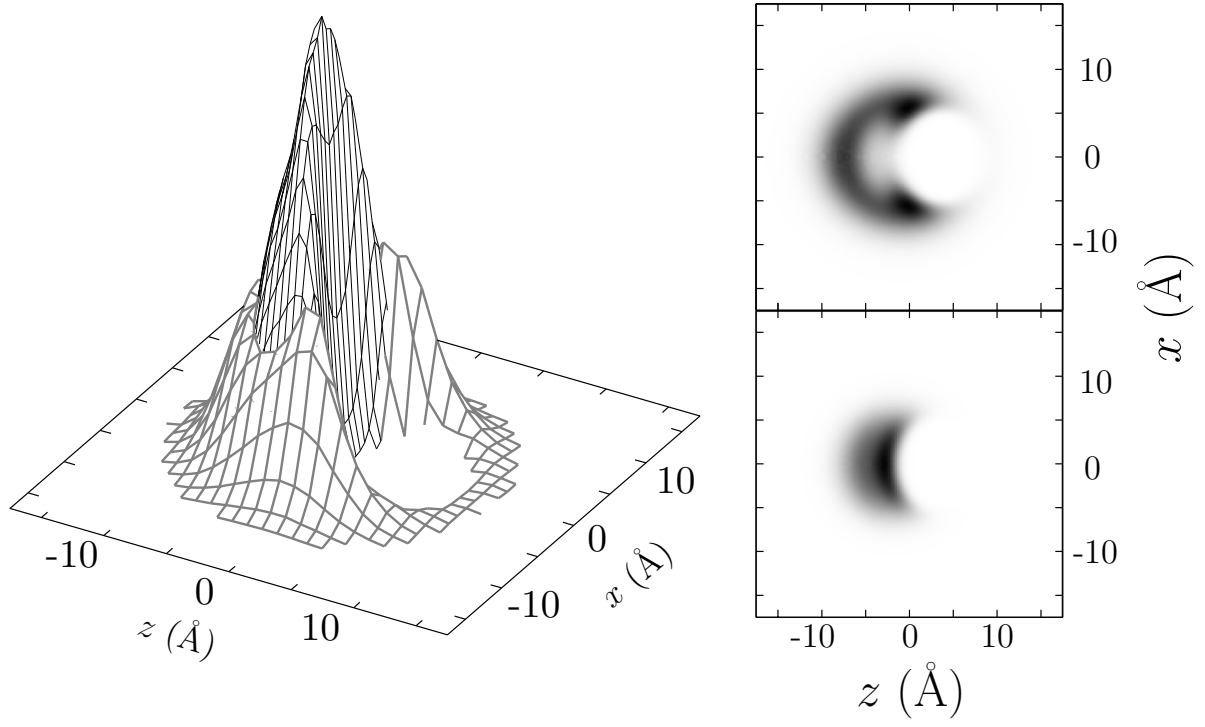


FIG. 4: Same as Fig. 1 for $N_4 = 8$, $N_3 = 8$.

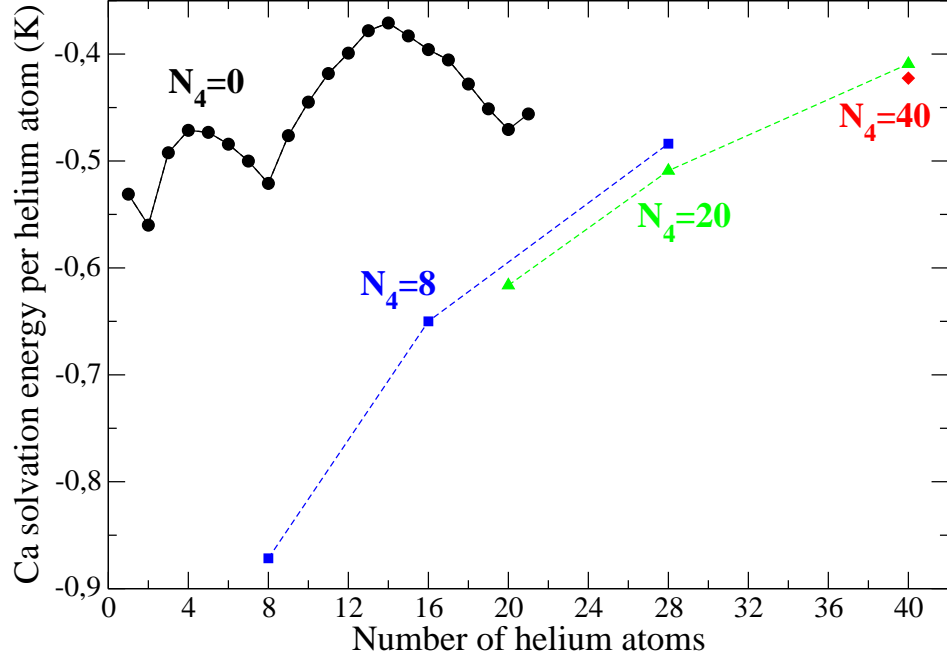


FIG. 5: (color online) Solvation energy of Ca per helium atom for several $\text{Ca}@^4\text{He}_{N_4}+^3\text{He}_{N_3}$ clusters, and total energy per helium atom of $\text{Ca}@^3\text{He}_{N_3}$ as a function of the total number of helium atoms in the cluster.

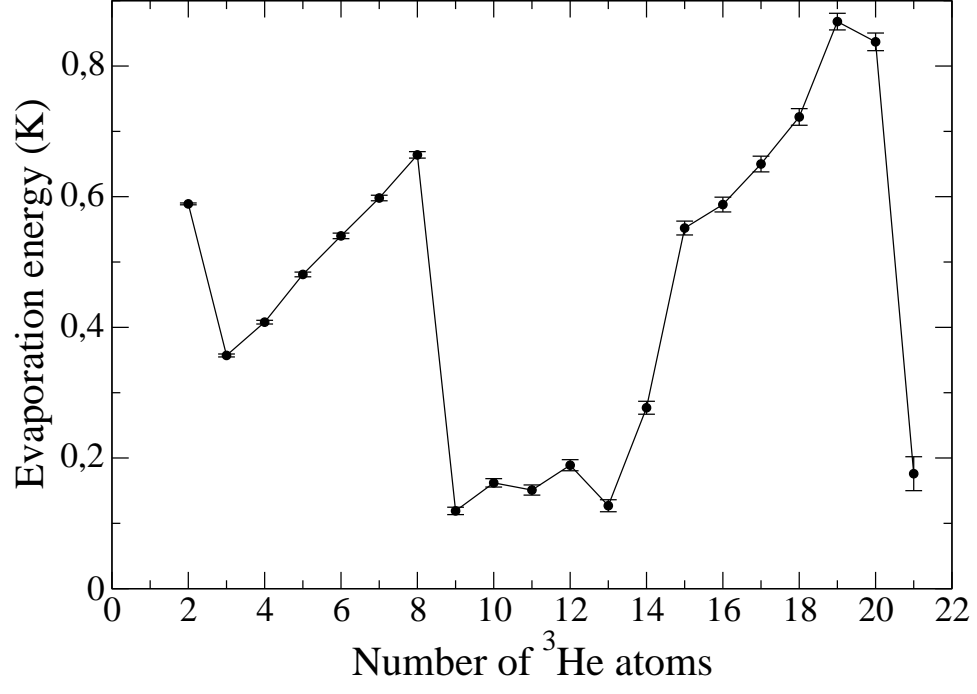


FIG. 6: Evaporation energies of ^3He atoms in $\text{Ca}@^3\text{He}_{N_3}$ clusters for the indicated N_3 values.

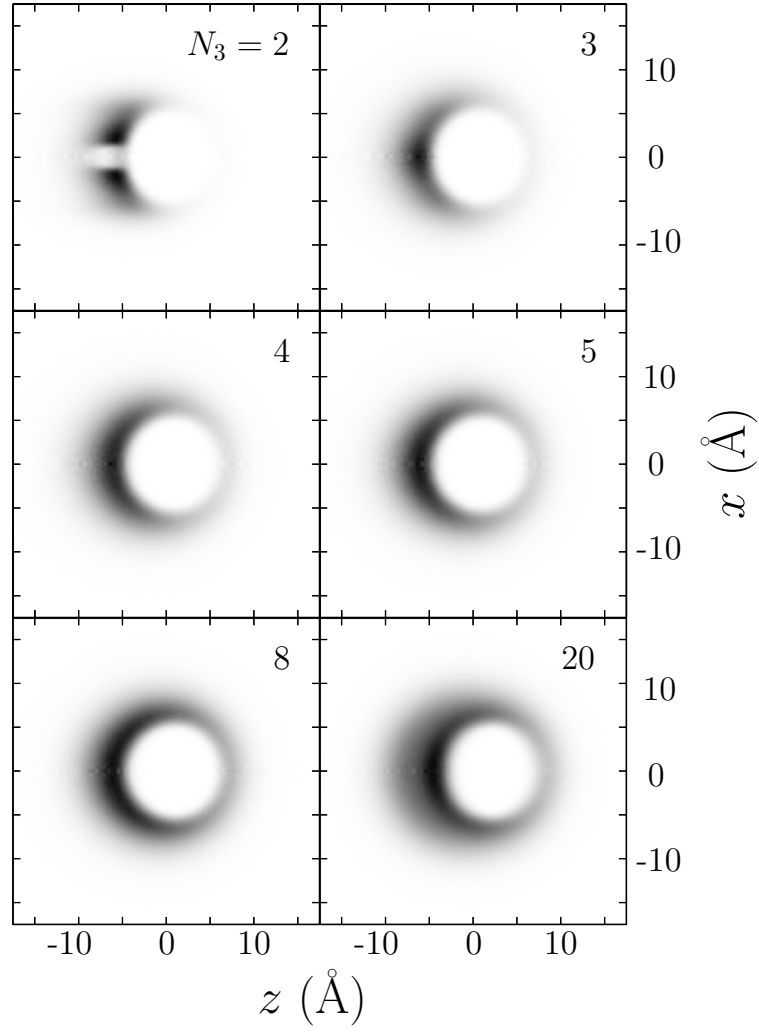


FIG. 7: Grey scale plot of the density distributions in the $y = 0$ plane for Ca@³He_{N₃} clusters with $N_3 = 2, 3, 4, 5, 8$, and 20 .

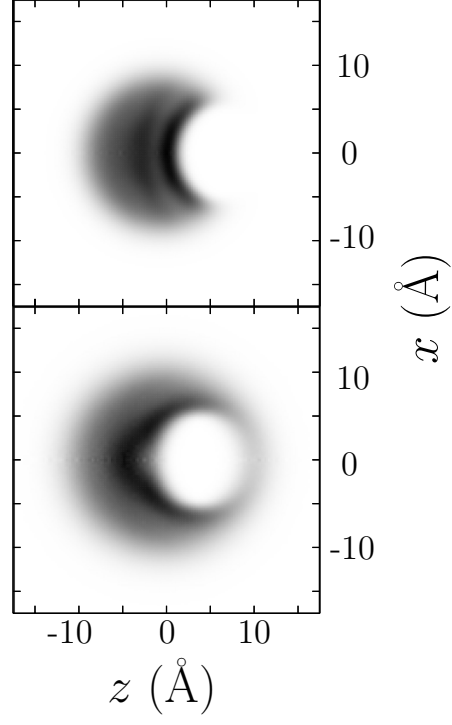


FIG. 8: Grey scale plot of the density distributions in the $y = 0$ plane for $\text{Ca@}^4\text{He}_{40}$ and $\text{Ca@}^3\text{He}_{40}$.

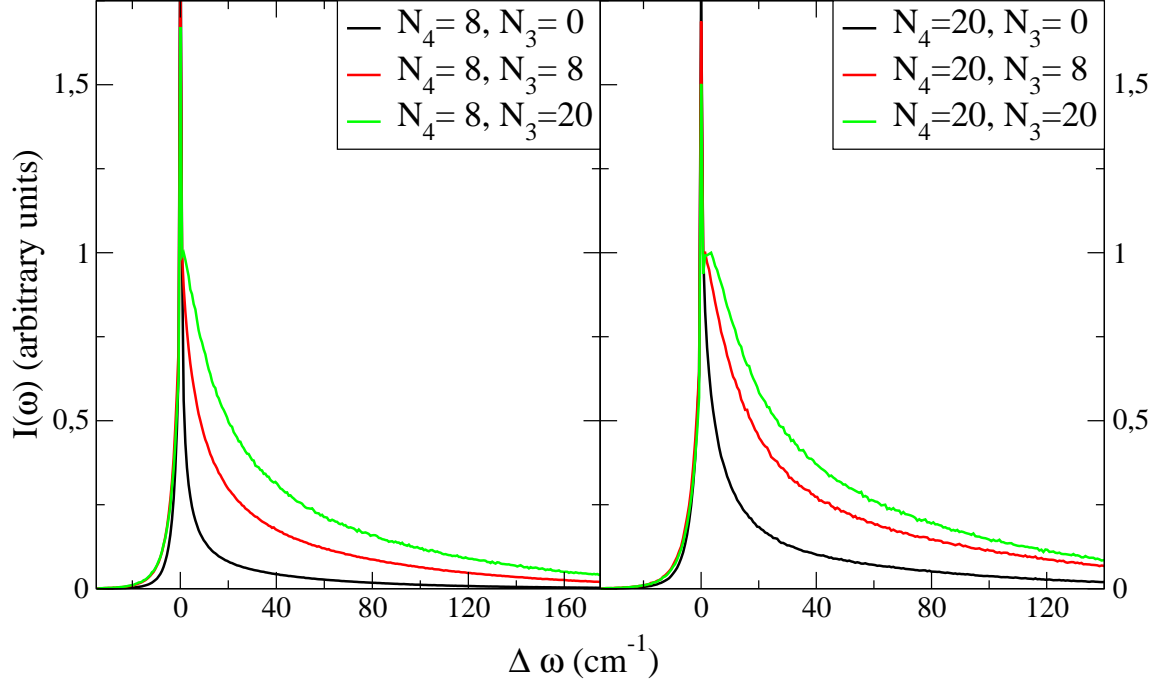


FIG. 9: (color online) Absorption spectrum of Ca in mixed clusters with $N_4 = 8$ (left panel) and $N_4 = 20$ (right panel), and three N_3 values.

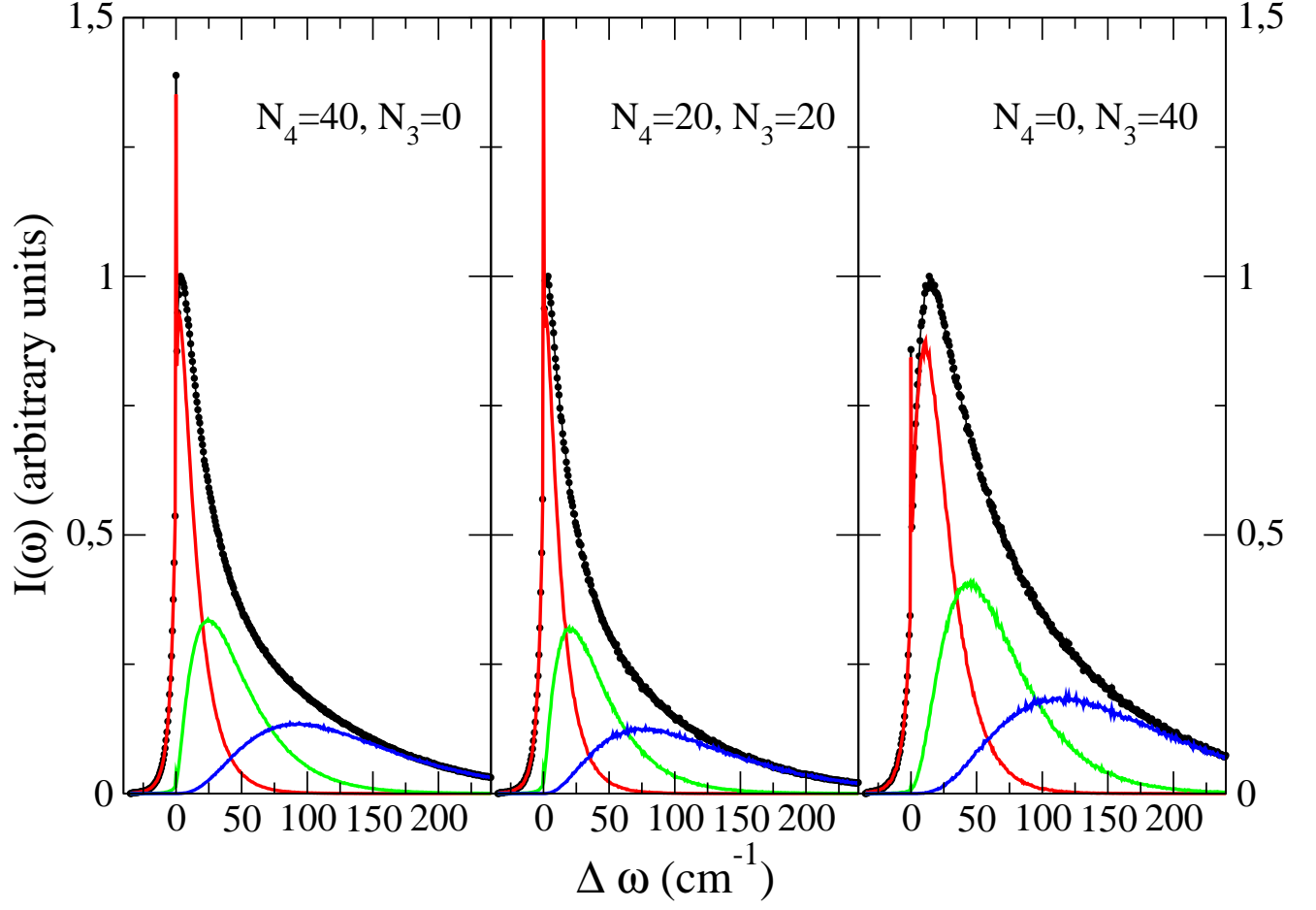


FIG. 10: (color online) Absorption spectrum of Ca for three selected combinations of helium atoms in clusters with $N_4 + N_3 = 40$.

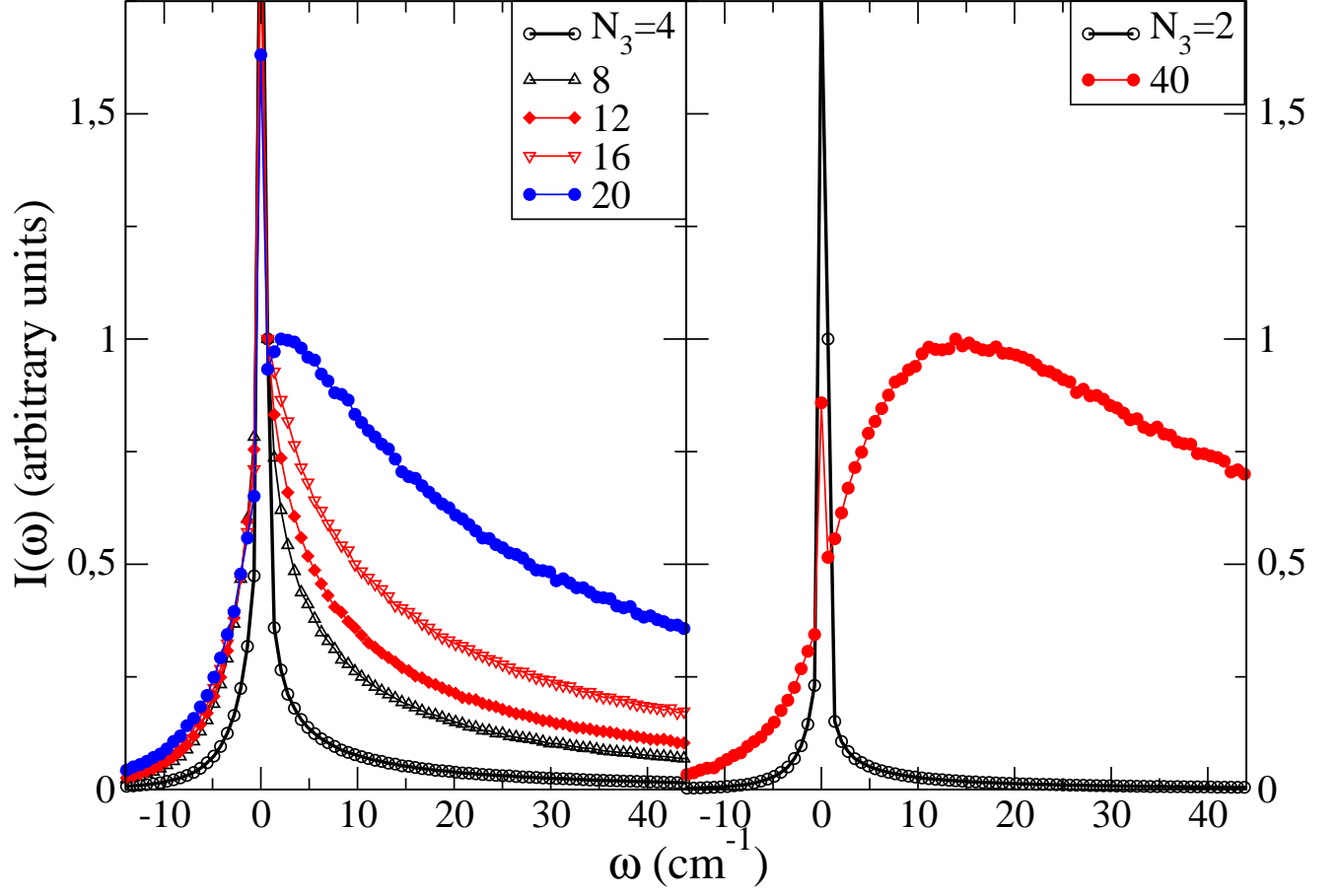


FIG. 11: (color online) Absorption spectrum of Ca in ${}^3\text{He}_{N_3}$ clusters for the indicated number of atoms. For clarity, the $N_3 = 2$ and 40 results have been drawn in a separate panel.